Earth Systems and Environment
https://doi.org/10.1007/s41748-018-0049-7

ORIGINAL ARTICLE

Estimating the Mean Circulation and Water Exchange of the Gulf of Suez-Red Sea via a Validated One-Way Atmospheric-Hydrodynamic Coupled Model

Ahmed Eladawy[1] · Mohamed Shaltout[2,3] · Magda Catarina Sousa[4] · João Miguel Dias[4] · Kazuo Nadaoka[5]

Received: 22 November 2017 / Accepted: 2 May 2018

Abstract
The Gulf of Suez, Northern Islands protected area, and Hurghada zone are experiencing mega developments in all sectors including tourism, industry, and logistics. The need for moderately accurate near-shore hydrodynamic models is increasing to support the sustainable development of this oceanic area. This can be accomplished by following a nesting approach including the downscaling of global atmospheric and oceanic models into local models using higher resolution datasets. This work aims to present the development of a one-way coupling between atmospheric and hydrodynamic models for the Gulf of Suez (GOS) to understand the local oceanic characteristics and processes. The Regional Climate Model system (RegCM4) is used to simulate moderate resolution atmospheric features and its results are used to force a local dedicated application of Delft3D model. The results indicate that the predicted water level, water temperature, and evaporation accurately follow in situ measurements, remotely sensed data, and re-analysis data. The results suggest that the annual sea surface temperature is averaged at 23 °C, while the annual average of evaporation rates equals 8.02 mm/day. The study suggests that the water level displays a marked seasonal and spatial variation. Moreover, the water balance in the Gulf of Suez was controlled by the difference between inflows and outflows through the Straits of Gubal and by the net precipitation. In addition, the water balance indicated a net loss of approximately 3.9×10^{-3} m of water during 2013. Moreover, the exchange through the Straits of Gubal showed a two-way exchange with a net inflow of 0.0007 Sv, where the outflow dominated in the surface layer along the western coast and the inflow dominated in the lower layers along the middle of the Straits. To conclude, the one-way coupling modeling technique proved to be a reliable tool for studying local features of the GOS region.

Keywords Northern Red Sea · Gulf of Suez · Atmospheric modeling · Hydrodynamic modeling · RegCM4 · Delft3D

1 Introduction

The GOS, which extends about 300 km from Port Suez in the north to Shadwan Island in the south, is connected to the northwestern Red Sea through the Straits of Gubal and to the Mediterranean Sea through the artificial Suez Canal (Fig. 1). The GOS is a semi-enclosed shallow basin with an average depth of 40 m, bounded by the Sinai Peninsula on the east and the eastern desert of Egypt on the west with a total surface area of about 10,510 km^2. The GOS, including Northern Islands protected area and Hurghada zone, is experiencing mega developments in all sectors, including tourism, industry, ports, and logistics. Moreover, the GOS is used for shipping, linking the Mediterranean Sea with the Red Sea via the artificial Suez Canal. Suez Canal is one of the world's most heavily used shipping lanes, as it is considered as the shortest maritime route between Europe and

✉ Ahmed Eladawy
ahmed.eladawy@ejust.edu.eg

[1] Irrigation & Hydraulics Department, Faculty of Engineering, Mansoura University, Mansoura, Egypt

[2] Oceanography Department, Faculty of Science, Alexandria University, Alexandria, Egypt

[3] Marine Science Department, Gothenburg University, Gothenburg, Sweden

[4] CESAM, Departamento de Física, Universidade de Aveiro, 3810-193 Aveiro, Portugal

[5] Department of Transdisciplinary Science and Engineering, School of Environment and Society, Tokyo Institute of Technology, Tokyo, Japan

Published online: 10 May 2018

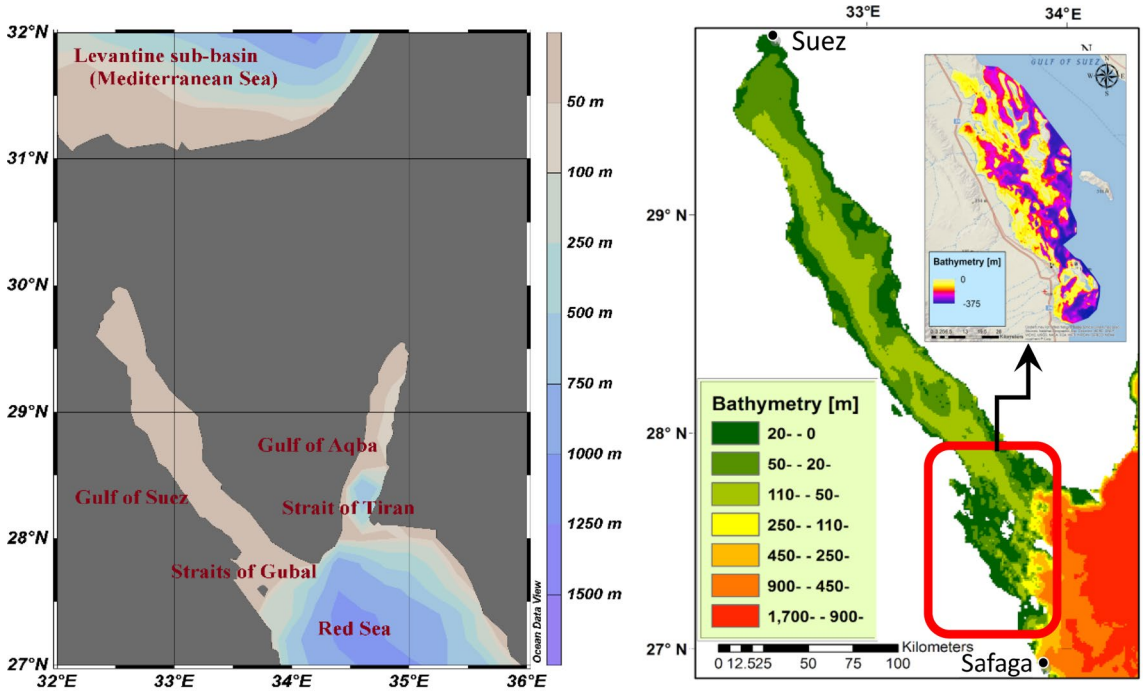

Fig. 1 Geographical location of the Gulf of Suez (left) together with the bathymetric map of the study area. Zoomed area is high resolution (30 m) Landsat 8 imagery-based bathymetric GIS data package for the shallower areas through the Straits of Gubal

South Asia. In addition, the GOS has a wide diversity of coral reefs and an excellent underwater aquatic life (Barakat et al. 2002), increasing its economic importance.

High shipping traffic and pollution through oil refineries, oil spill power stations, and domestic drainage (Hamed and Emara 2006) in the study area together with limited scientific literature and lack of ocean measurements recently boost the interest of oceanographers to start modeling the oceanic characteristics of the GOS. Some earlier relevant studies focusing on the local oceanic features are available, but are limited in the understanding and characterization of this area. As a part of the Northern Red Sea weather system, the sea level pressure patterns over the NRS showed a smooth pattern which decreased the wind speed (Eladawy et al. 2017). The sea level pressure decreased from its higher values over the Levantine Basin (southeastern basin of the Mediterranean Sea) to its minimum values to the Gulf of Aden to the south. The surface wind was roughly parallel to the isobars in a clockwise direction around high pressure. This indicates that the geostrophic wind direction over the NRS blew towards the southeast and was parallel to the Red Sea's axis (Abualnaja et al. 2015; Papadopoulos et al. 2013). The local tidal characteristics were considered by Rasul and Stewart (2015) who found that the tide in GOS is mainly diurnal, with a tidal range of 60 cm at the Straits of Gubal. Morcos (1970) studied the local evaporation, finding that the loss of water from the gulf system largely exceeds the combined gains from precipitation and runoff (through flash floods). Based on a previous application of Delft3D modeling system, Madah et al. (2015) stated that the Red Sea, in general, is characterized by a weak tidal current except at the Strait of Bab-el-Mandeb and Gulf of Suez. According to Maillard (1974), Wyrtki (1974), Maillard and Soliman (1986), Cember (1988), and Woelk and Quadfasel (1996), the primary source of the Red Sea Deep Water (RSDW) is the Suez Gulf with an annual formation rate of about 0.04 Sv. The relatively low water temperature and continuous evaporation in the GOS lead to the formation of dense water that turn under and is returned southward initiating the RSDW. Generally, the prevailing wind direction (NW) over the Gulf of Suez enhances the surface outflow during winter (September–June) as described by Al Gain et al. (1987). These findings run counter Rady et al. (2000) results. These authors applied a three-dimensional non-linear hydrodynamic numerical model to show that the GOS is characterized by a typical (quasi) baroclinic two-layered inverse-estuarine circulation; the surface (lower) currents flow in the northwest (southeast) direction. Moreover, they also stated that the deep outflow from the GOS to the Red Sea is estimated to be 0.058 Sv, most markedly during winter. Generally, there is a lack of long-term observations at the GOS (Towers 2015), which results in uncertainties on the studies performed until now about the GOS circulation. The one-way coupling model technique's application can contribute

to overlap these limitations and help to understand the exchange patterns through the Straits of Gubal, which is the main aim of the present work.

Many oceanographers actually use the two-way coupling between atmospheric and ocean models to simulate local oceanic features (Bye 1996; Woolnough et al. 2007; Watterson and Syktus 2006). However, the one-way coupled ocean model (forced by the atmosphere model) also proved to be a relevant tool to study ocean characteristics, and in some cases, gives better results than the two-way coupling technique (Ličer et al. 2016). Many other oceanographic modelers use 3D oceanic models as standalone models forced by an atmospheric component to model local oceanic characteristics [e.g., MITgcm (Adcroft et al. 2014; Yao et al. 2014), HYCOM (Bower 2002; Chassignet et al. 2007), ROMS (Shchepetkin and McWilliams 2005), and Delft3D (Hydraulics 2011)]. Other oceanic modelers directly model the oceanic characteristics forced by re-analyzed data as a relevant way to shape the general features of the ocean (Calmanti et al. 2006; Shaltout and Omstedt 2015).

Considering the increasing need for a solid understanding of the Gulf of Suez (GOS) circulation patterns, the development of an accurate hydrodynamic model for this region is of utmost relevance. Therefore, in this work, the first application of an atmospheric-ocean regional climate model for the Gulf of Suez is presented. This uses a one-way coupled ocean model technique, where the Delft3D oceanic model is forced by the RegCM4 atmospheric regional climate model to understand the oceanic physical characteristics of the GOS over the year 2013. The model simulations are validated and the main conclusions are drawn using independent oceanographic databases.

In detail, this work aims to (1) examine the physical characteristics of GOS including water levels, water temperature, and evaporation, (2) explore the water balance of the GOS, (3) study the exchange characteristics between the GOS and Northern Red Sea through the Straits of Gubal, and (4) describe the depth-averaged circulation of GOS.

2 Data and Methodology

2.1 Data Used

The data used here to assess the water and heat balances as well as GOS general circulation include:

Data used for RegCM4

1. Data on air temperature (*T*), geopotential height (hgt), relative humidity (*RH*), and two wind components (*U* and *V*) at 27 different pressure levels were extracted from the European Centre for Medium-Range Weather Forecasts (ECMWF; http://data.ecmwf.int/data/) with a 3-h temporal resolution and a spatial resolution of 0.75° × 0.75° (ERA-Interim).
2. Surface topography data (GTOPO30) and surface land use datasets of 12 km spatial distribution. These datasets were obtained from the ICTP RegCM4 database (http://users.ictp.it/~pubregcm/RegCM4/globedat.htm#part5).
3. Sea surface temperature (ERSST) with 0.75° × 0.75° spatial resolution and 6-h temporal resolution were extracted from ICTP RegCM4 database http://users.ictp.it/~pubregcm/RegCM4/globedat.htm#part5

Data used for Delft3D-FLOW

1. Data on sky cloudiness, net downward shortwave, surface air temperature, surface wind components, and air pressure were obtained from the current result of RegCM4 simulation.
2. Bathymetric map of the GOS extracted from the EMODnet digital terrain model (DTM) that was created with a resolution of about 230 m (http://portal.emodnet-bathymetry.eu/help/help.html).
3. High resolution (30 m) Landsat 8 imagery-based bathymetric GIS data package for the shallower areas of Northern Islands and Hurghada area was purchased from TCarta Marine Bathymetry GIS. The data are combined with nautical charts. In addition, a 1:20,000 scale shoreline was provided (http://www.tcarta.com/home/landsat-derived-bathymetry/).
4. Tidal conditions south to the open boundary were obtained from TPXO 7.2 global inverse tide model via Delft Dashboard GUI (http://volkov.oce.orst.edu/tides/global.html)
5. Depth-time varying profiles for salinity and water temperature south to the open boundary were obtained from HYCOM model results (https://hycom.org/dataserver/).

Data used for validation

1. Hourly measured data of 2 m air temperature, air pressure, cloud cover, and surface wind components over Suez (29°58.040′N, 32°33.012′E), and Safaga (26°46.523′N, 33°56.417′E) were used to verify the RegCM4 simulations.
2. Remotely sensed daily ocean wind data were extracted freely from the Advanced Scatterometer (ASCAT)'s wind maps (Bentamy and Fillon 2012), (ftp://ftp.ifremer.fr/ifremer/cersat/products/gridded/MWF/L3/). The ASCAT data were processed by the National Oceanic and Atmospheric Administration (NOAA) which utilizes measurements from ASCAT aboard the EUMETSAT METOP satellite on the C-band (Chang et al. 2015). These data have a spatial resolution of 0.25° in longitude and latitude.

3. Hourly water levels observed at two stations [Shadwan Island (27.471°N, 34.012°E) and Zafarana locations (29.036°N, 32.687°E)] are used to examine the representative water levels in the coastal areas. These data are available through Delft Dashboard (https://publicwiki.deltares.nl/display/DDB).
4. Gridded daily AVHRR data (version 2) with a 0.25° spatial resolution for 2013 (http://www.ncdc.noaa.gov/oa/climate/research/sst/griddata.php) was used to examine the predicted sea surface temperature accuracy.
5. A 3-D profile of water temperature was obtained from the World Ocean Atlas 2013 version 2 (hereafter, WOA 2013) to verify the 3-D simulation of water temperature (https://www.nodc.noaa.gov/OC5/woa13/).

2.2 One-Way Coupling System (Delft_Reg_GOS.0.1)

2.2.1 Atmospheric Modeling (RegCM4)

RegCM is a regional climate model developed for long-term regional climate simulations (Giorgi et al. 2012). RegCM4 (the version which is used in the present study) gives better flexibility, portability, and user-friendliness than the previous generation RegCM3. RegCM4 is an effective tool for downscaling of atmospheric/climate characteristics over a wide range of spatial area (Giorgi and Mearns 1999; Giorgi 2006; Qian 2008; Qian et al. 2010).

RegCM4 is a hydrostatic and compressible model that uses sigma-P vertical coordinates together with the dynamic core of MM5 (Grell et al. 1994). The current version of RegCM4 employs: (1) the radiative transfer scheme of the global model CCM3 (Kiehl et al. 1996) for calculating the radiative transfer, (2) Holtslag scheme (Holtslag et al. 1990) to describe the planetary boundary layer, (3) Grell scheme (Grell 1993) for representing cumulus convection, (4) SUBEX scheme (Pal et al. 2000) as a resolved scale precipitation, (5) the Biosphere–Atmosphere Transfer Scheme (Dickinson et al. 1993) to describe land surface processes, and (6) the Zeng scheme (Zeng et al. 1998) to describe ocean fluxes (for more details see Giorgi and Anyah 2012).

The atmospheric simulations are conducted over a domain (26°–31°N, 31°–35°E) encompassing the GOS, the surrounding area, and the buffer zone. This simulation is performed using a spatial resolution of 12 km and 18 sigma-P vertical levels for 2 years (2012–2013). The results of the first year (2012) are used as spin-up; the year 2013 is coupled with Delft3D.

2.2.2 Hydrodynamic Ocean Modeling (Delft3D-FLOW)

The Delft3D-FLOW model is widely used as a hydro-environmental tool to perform oceanic studies across the globe. As an example, a three-dimensional hydro-environmental model of the Arabian Gulf (AG) was developed based on the Delft3D-FLOW model and Delft3D-WAQ model (Pokavanich et al. 2014). This model was also applied by van den Heuvel (2010) to study the impact of the diversion scenarios on salinity (gradients) on Pontchartrain Basin. Another application was developed to assess the large-scale water temperature cycle of the South China Sea considering significant spatial and temporal scales (Twigt 2006).

Delft3D is an open source model that is world-renowned, which can be used in two- and three-dimensional modeling modes to investigate hydrodynamics, sediment transport, morphology, and water quality. Delft3D-FLOW is the hydrodynamic module that solves the unsteady non-linear shallow-water equations in three dimensions with a hydrostatic assumption resulting from tidal and meteorological forcing on a curvilinear, boundary-fitted grid. The model includes: tidal forcing, Coriolis forces, density-driven flow (pressure gradient terms in the momentum equations), an advection–diffusion solver to compute density gradients with an optional facility to treat very sharp gradients in the vertical space and time, varying wind and atmospheric pressure, advanced turbulence models to account for the vertical turbulent viscosity and diffusivity based on the eddy viscosity concept (Roberts et al. 2015).

Delft3D-FLOW model equations are solved by applying sigma layering vertically, and in this study, the model runs in the 3D mode (Hydraulics 2006, 2011). The Delft3D-FLOW hydrodynamic model was implemented to simulate the water levels and current's field in the GOS. The model domain has a horizontal resolution of 1.1 km and 15 vertical sigma layers expanding from the surface to bottom. Delft3D-FLOW model was forced at the open boundary (Fig. 2) using the HYCOM results for daily profiles of water temperature and salinity. Moreover, tidal conditions at the open boundaries are extracted from the Topex dataset (TPXO 7.2) which contains data on 13 tidal constituents on a global 0.25° grid (Egbert and Erofeeva 2002; Egbert et al. 1994). In addition, atmospheric forcing [such as wind at 10 m (U10 and V10), air temperature at 2 m (*T*2 m), relative humidity (rh), cloud cover (tcc), total precipitation (Tp), and sea level pressure (*SLP*)] are taken via the one-way coupling with the developed RegCM4 model outputs in hourly basis. The initial conditions of GOS (initial profiles of water temperature and salinity) are taken on January 1 2012 from HYCOM results. Linear interpolation is used to coincide with the vertical levels from HYCOM results and Delft3D-FLOW. Wind drag coefficients are calculated linearly from 0.00063 to 0.0027 at wind speeds of 0 and 25 m/s, respectively. The turbulence model chosen for the current study is the k–Ɛ 3D-turbulence closure (Hydraulics 2014). Manning coefficient was set to 0.02 ($s/m^{1/3}$) and was used for the calculations of the constant bottom roughness friction coefficient. Two different heat flux schemes are available within Delft3D-FLOW

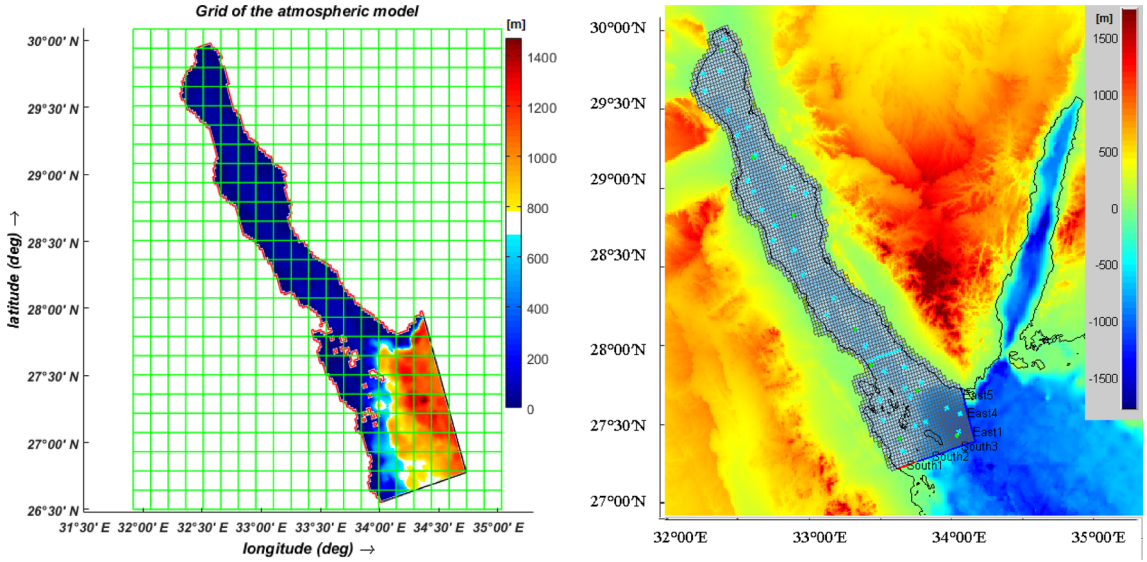

Fig. 2 The grid of the RegCM4 simulation (left) together with Delft 3D grid including the location of the oceanic open boundary (right). The bathymetry and digital elevation model (DEM) data are included in meters

model: Murakami scheme (Murakami et al. 1985) and the ocean model scheme (Lane 1989). These two schemes were tested, and the most efficient in describing the heat flux daily cycle over GOS was found to be the ocean model which was then used in the current study.

The present version of the one-way coupling between RegCM4 and Delft3D-FLOW (hereafter, Delft_Reg_GOS.0.1) runs to simulate heat and water balances together with the current field of GOS over the years 2012–2013 (2012 is considered as the spin-up year). The coupling frequency is 1 h, and the study area was expanded south of the Straits of Gubal to provide a relaxation area between open boundary conditions and GOS. The exchange through the Suez Canal is neglected as it is considered much smaller than the exchange through the Straits of Gubal. Thus, the only open boundary conditions are at the south of the straights of Gubal (Fig. 2), where 3-h HYCOM vertical water temperature and salinity profiles along six segment sections well-distributed along the open boundary were imposed (Fig. 3). Table 1 shows the spatial average tidal constituents that were applied at the open boundary segments. Finally, the Delft_Reg_GOS.0.1 model framework is illustrated in Fig. 4.

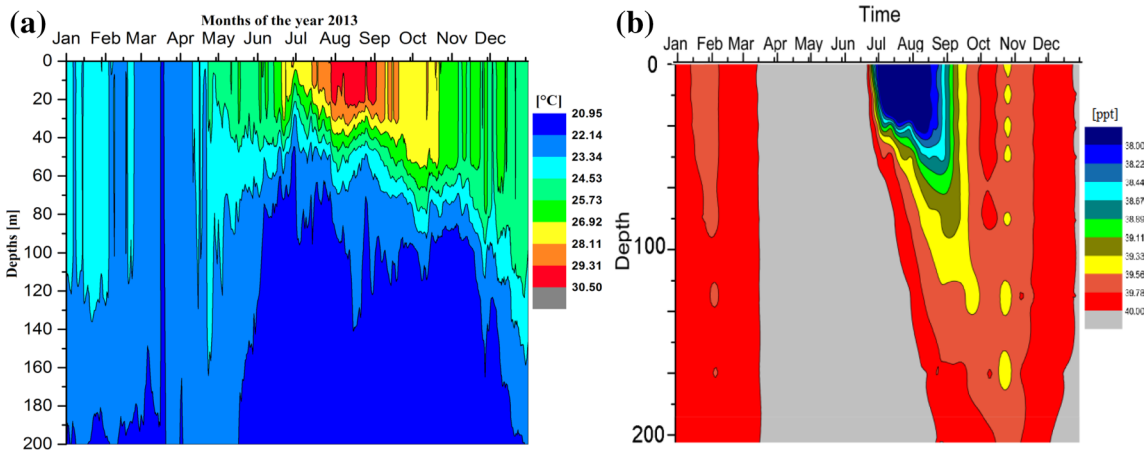

Fig. 3 Sample of the applied depth varying conditions for daily water temperature (**a**) and salinity (**b**) used at one point (27.419°N, 34.116°E) of the open boundary segments of the model for the entire year 2013

Table 1 Tidal constituents imposed at the open boundary segments

Constituents	M2	S2	N2	K2	K1	O1	P1	Q1	MF	MM	M4	MS4	MN4
Amplitude ($10^{-2}\times$m)	24.5	5.52	8.14	2.46	2.52	0.771	0.153	0.750	0.468	0.244	0.317	0.099	0.033
Phase (°)	121	141	95.4	143	127	119	90.3	197	131	98.1	135	50.7	258

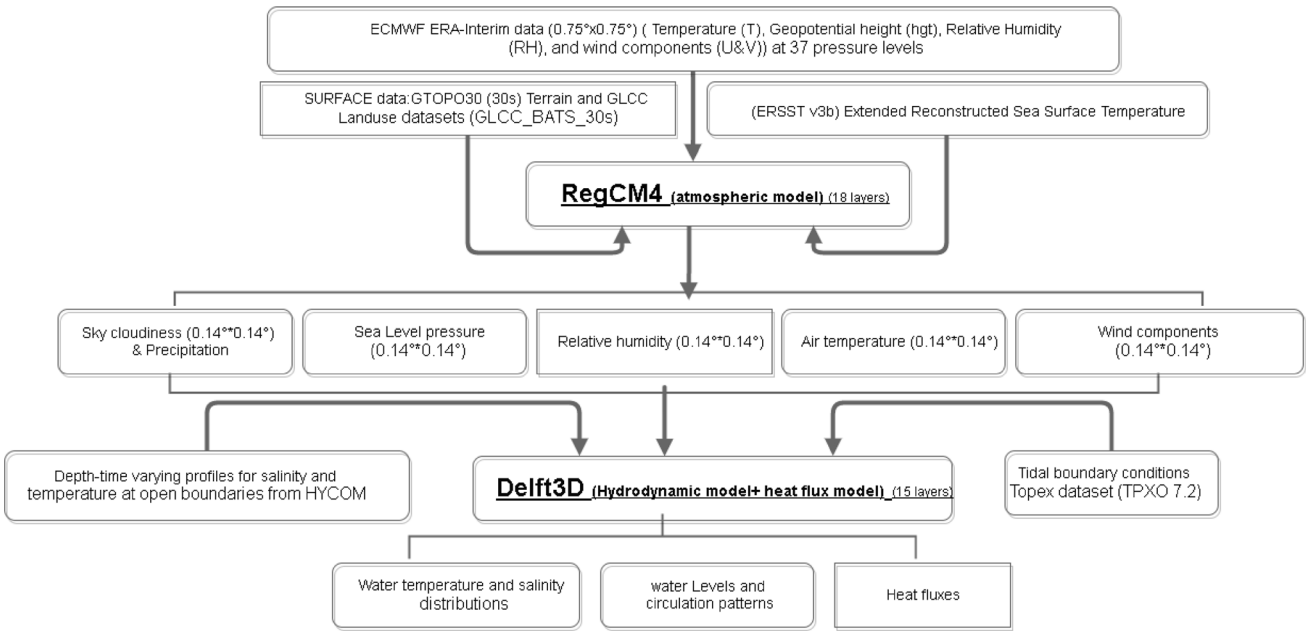

Fig. 4 Framework of the study

3 Results and Discussion

3.1 RegCM4

3.1.1 RegCM4 Verification

RegCM4 results were compared with the available observations and remotely sensed data to check the accuracy of its simulations over the years 2013–2014. The observed atmospheric data are available for two cities: Suez and Safaga (Fig. 1). RegCM4's hourly predictions of *T*2 m reproduce well the observed values over both stations and demonstrate considerable skill in reproducing the drops in *T*2 m values (e.g., during the middle of December 2013) as seen in Fig. 5. RegCM4 underestimated hourly *T*2 m by 0.13 °C over Suez (significant correlation coefficient, $R = 0.89$) while over Safaga an overestimation of 0.93 °C was found (significant correlation coefficient, $R = 0.92$). The two points used for the model verification are close to the seaside, where the *SST*s have more pronounced controls on climate. In addition, the slight discrepancies found may be due to the difference between the heights from the ground where the parameters are measured and the heights where the model predictions were extracted.

Another test performed to assess the accuracy of RegCM4 model's surface wind predictions of the over GOS considered the comparison between hourly model predictions and measured surface wind over Suez and Safaga stations. There is a reasonable agreement between the RegCM4 predictions and observed surface wind (Fig. 6). Moreover, RegCM4's daily surface wind predictions show better accuracy than the remotely sensed ASCAT for the surface wind over Suez and Safaga stations. This indicates that the RegCM4 results are the best alternative to be used in the one-way atmospheric-hydrodynamic coupled model with Delft3D, given the excellent spatial and temporal availability provided for the study area.

3.1.2 RegCM4 Results

The results of RegCM4 output including *T*2 m, rh, SLP, U10, V10, Tp, and TCC are shown in this section (Fig. 7).

The annual average *T*2 m over GOS ranged from 21 °C to 27 °C (Fig. 7a). *T*2 m increased southward, partly due to the effect of surface wind regime, surface thermohaline cyclonic

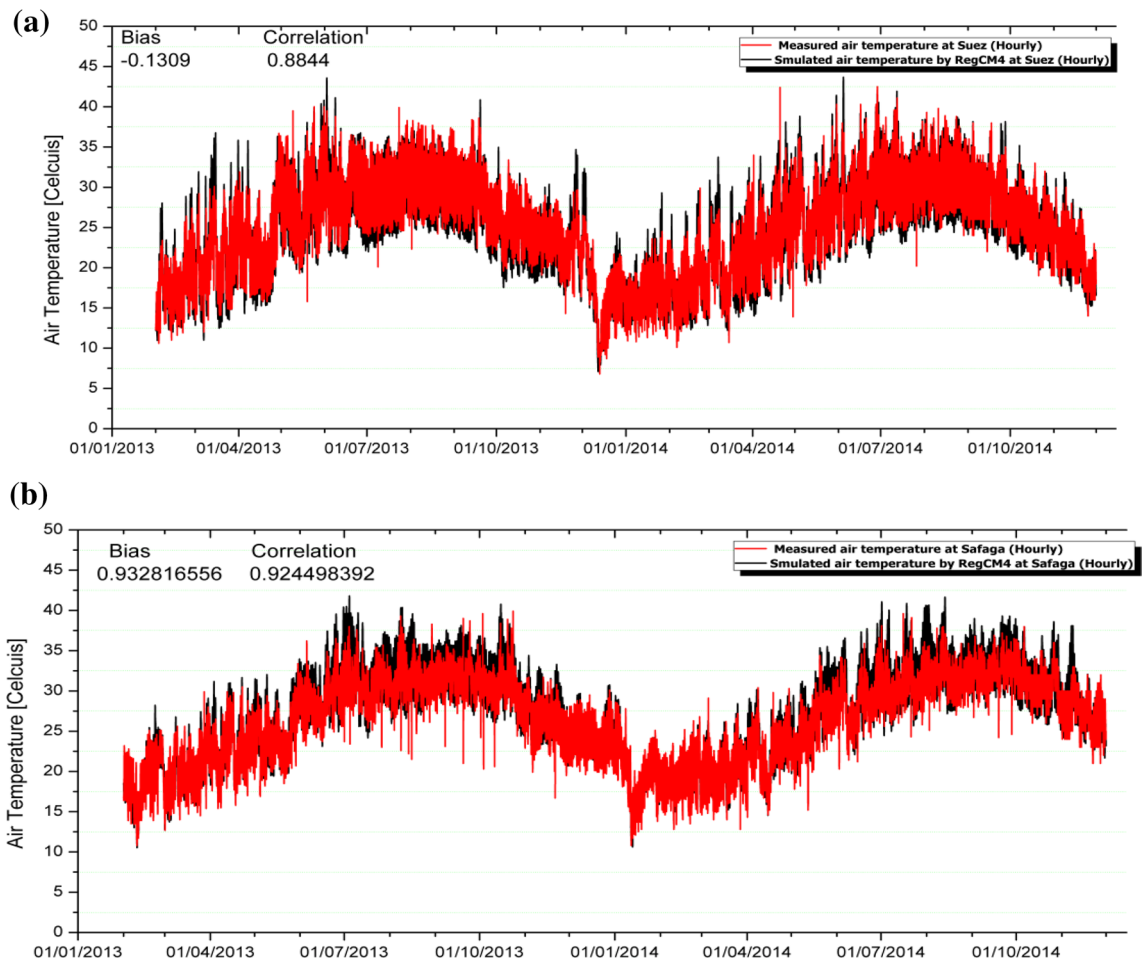

Fig. 5 Hourly measured and predicted surface air temperature (°C) at two stations (Suez (**a**) Safaga (**b**)) using RegCM4 model over 2013–2014

circulation, and the total heat loss from the atmosphere. The annual average rh (Fig. 7b) ranged from 30 to 50%. The maximum rh values occurred over the north GOS. However, the minimum value occurred over the southwestern area of the GOS. In addition, the annual average SLP ranged from 1013 mb (most markedly over the northwestern part of the GOS) to 1010 mb (most markedly over the southeastern part of the GOS); this partly indicates that the southwestern winds are dominant over the GOS. The smooth distribution of SLP indicates that the GOS is described with the weaker wind. The annual prevailing wind direction over the GOS (Fig. 7d) blows to a southeastern direction parallel to the Red Sea axis, partly due to the effect of mountains along the coastal areas. Moreover, the annual average wind speed over GOS is described by weaker wind speed ranging from 3 to 7 m/s, partly due to the smooth sea level pressure over GOS and the surrounding areas. Generally, the Tp range shows its maximum values (0.14 mm/day) over the northeastern GOS (Fig. 7e), indicating that the GOS is a dry region. The TCC pattern follows the Tp pattern well (Fig. 7f). The annual TCC ranges from 10 to 17%, corroborating the previous results that show GOS is characterized by a warm and drought atmosphere.

3.2 One-Way Coupling System (Delft_Reg_GOS.0.1)

3.2.1 Delft_Reg_GOS.0.1 Validation and Sensitivity

The Delft_Reg_GOS.0.1 model results were first examined by comparing predicted and measured water levels at two stations near Shadwan Island and Zafarana stations (Fig. 8). The predicted hourly water level reproduces the observations in the case of the Shadwan station, but there is a slight difference between water levels in the Ras Gharib station. The normalized root-mean-square-error (NRMSE) between predicted and observed water level was 7.53 and 12.81% at Shadwan and Zafarana stations, respectively. The model coarse resolution may introduce some local inaccuracies that make the predictions differ from actual tidal amplitude.

In addition, Delft_Reg_GOS.0.1 shows lower SST estimates of about 0.5 °C in comparison with Gridded daily AVHRR SST, most (less) markedly along southern and

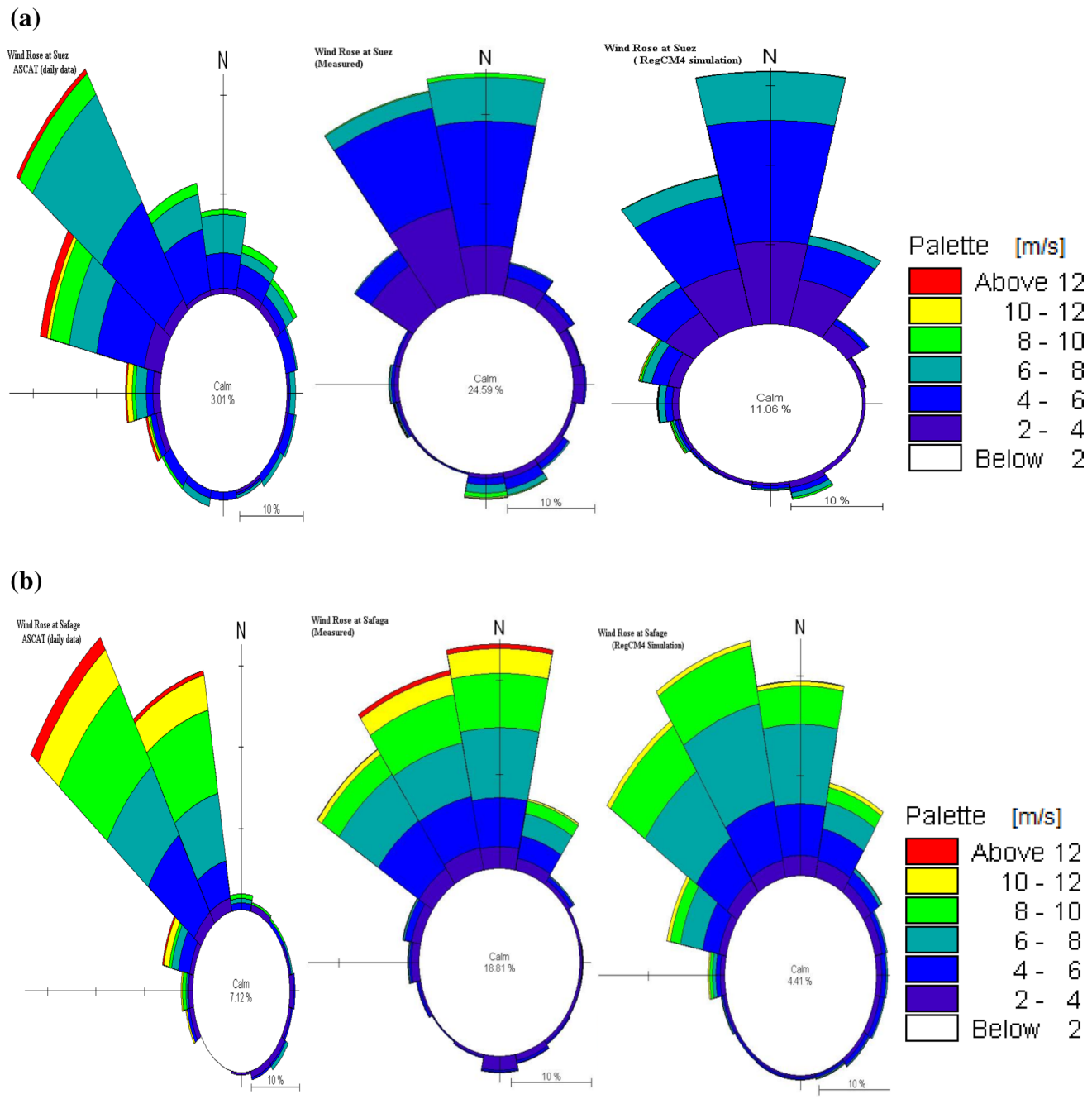

Fig. 6 Annual wind roses (wind speeds are in m/s) based on measured data (hourly), RegCM4 predictions (hourly), and ASCAT (daily) at Suez (**a**), and Safaga (**b**), over 2013–2014

western (northern) coast of GOS as seen in Fig. 9. Generally, Delft_Reg_GOS.0.1 SST shows seasonally lower estimate ranges from 0.1 °C during winter to 0.86 °C during summer. Generally, Delft_Reg_GOS.0.1 and AVHRR SST describe significant seasonal correlations ranging between 0.5 during winter and 0.94 during spring, with a significant annual correlation of 0.93 ($n = 365$; data not shown). Figure 10 presents the time series of predicted and WOA 2013 water temperature profile data for a station located south of the Straits of Gubal (34.1°E, 27.6°N) which represents the buffer zone. It can be concluded that the water temperature profile over the buffer zone is reasonably simulated by Delft_Reg_GOS.0.1, partly confirming that the k–Ɛ 3D-turbulence and mixed scheme adopted in this simulation works reasonably well in this model implementation. Due to the lack of information of WOA 2013 inside the GOS, water temperature profile verification was done only over the buffer zone.

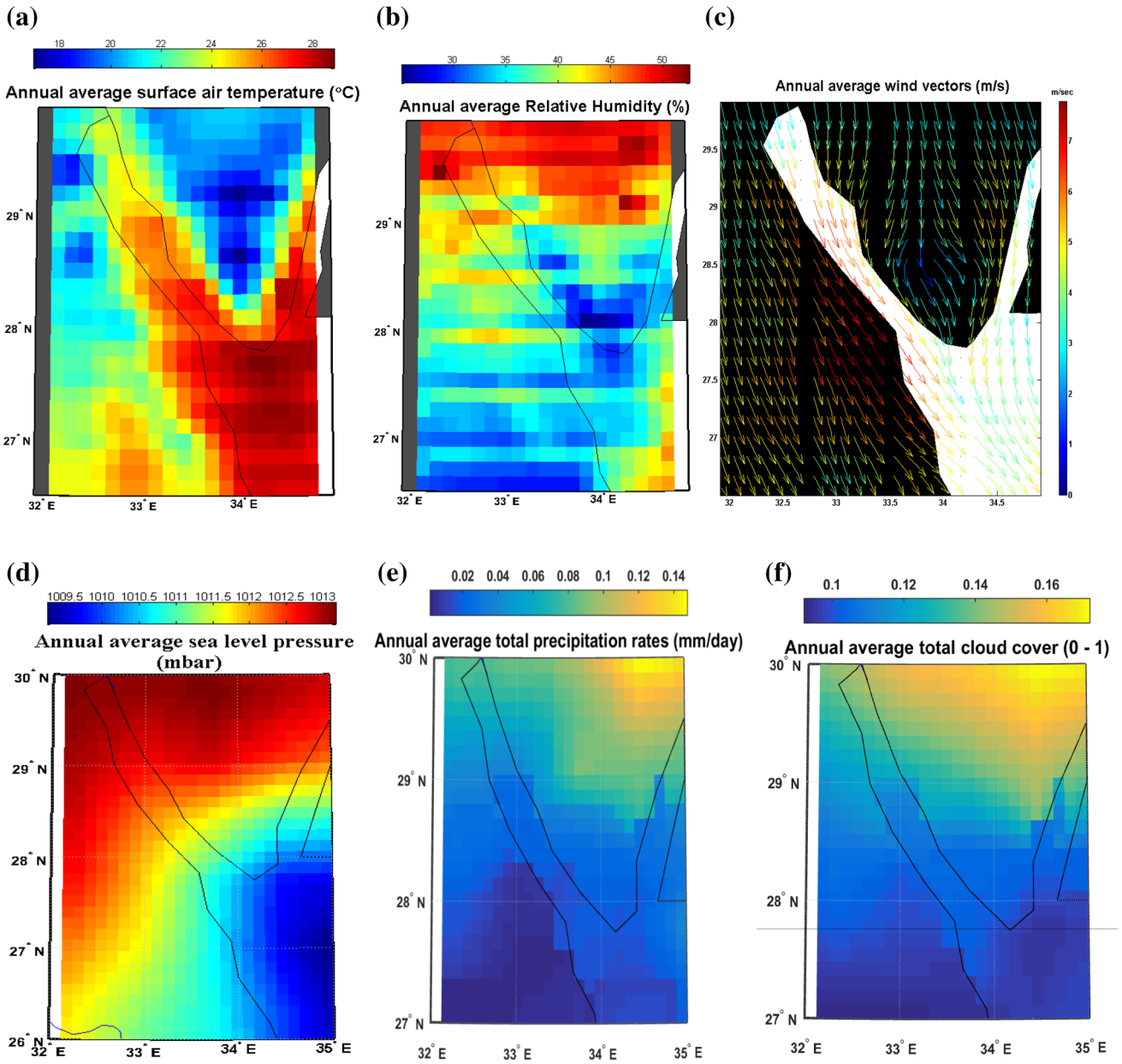

Fig. 7 Averaged annual (2013–2014) air temperature (°C) (**a**), relative humidity (%) (**b**), **c** wind streamlines, **d** sea level pressure (mbar) (**e**), annual average precipitation (mm/day) (**e**), and average annual total coverage (**f**) based on the hourly predictions of the RegCM4 model

To evaluate the modeling approach, the evaporation over GOS was simulated using the Delft_Reg_GOS.0.1, and its predictions were compared with ERA-Interim database. The comparison indicates a close annual correlation ($R = 0.7$, $n = 365$) with the predicted evaporation deviating approximately 25% from the ERA-Interim database value (data not shown), partly due to the coarse resolution of ERA-Interim (this database was calculated with $0.75° \times 0.75°$ resolution and then downscaled to $0.125° \times 0.125°°$ resolution using bilinear interpolation). This indicates that Delft_Reg_GOS.0.1 constitutes a reliable tool to study the evaporation within narrow ocean domains (e.g., GOS).

To analyze the sensitivity of the Delft_Reg_GOS.0.1 model to changes in lateral boundary conditions and atmospheric forcing, two sensitivity runs were performed by adding ± 1 °C to the vertical water temperature profiles at the lateral boundaries. Two additional sensitivity runs were carried out by adding ± 1 °C to the forcing $T2$ m (data not shown). It can be concluded that changes in vertical temperature profiles by $1(-1)$ °C modified the bias in GOS surface water temperature by $0.6(-1.1)$ °C especially near

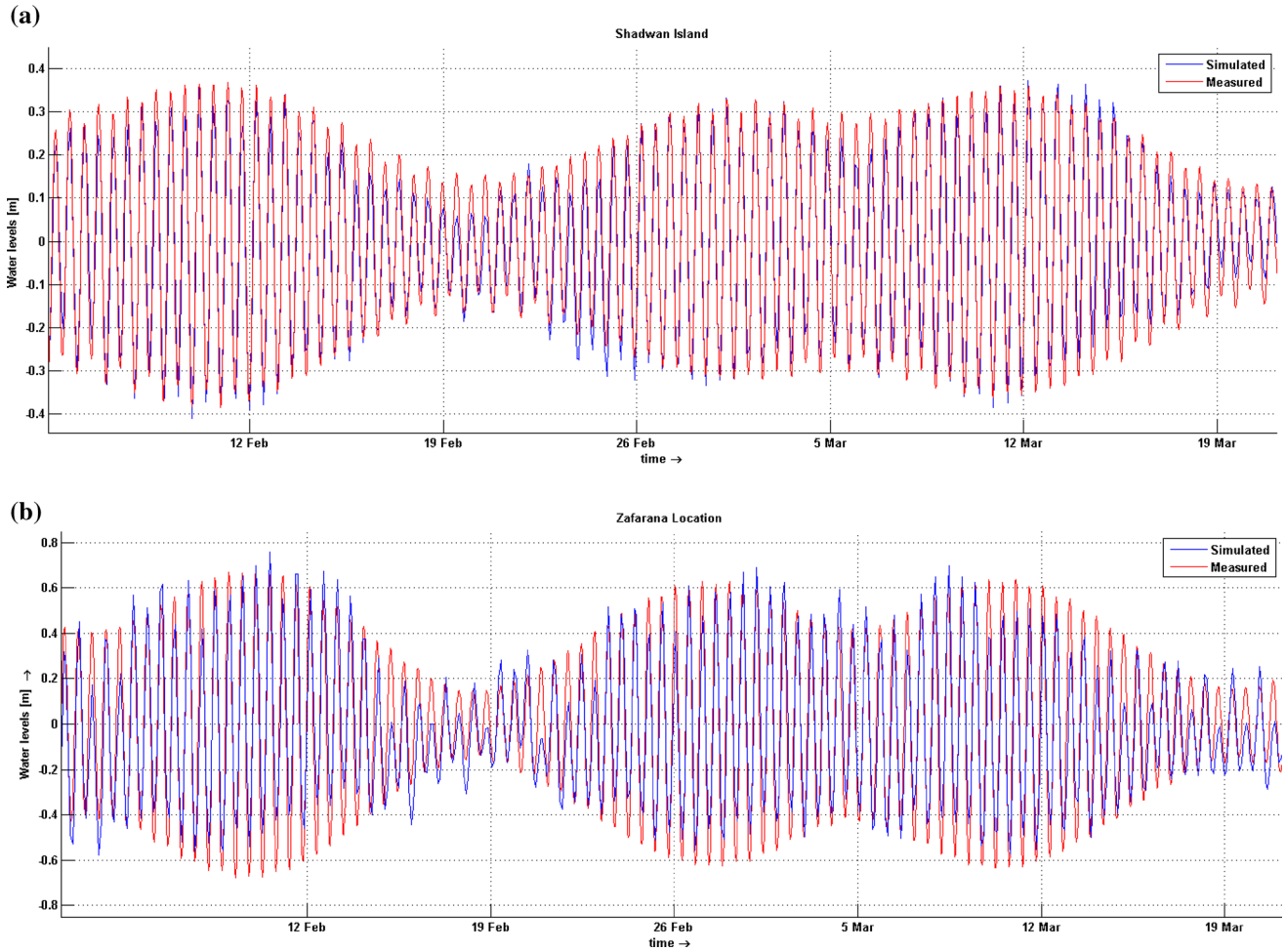

Fig. 8 Observed and predicted water level at Shadwan and Ras Gharib stations

the Straits of Gubal. Moreover, changing the forcing $T2$ m by 1(− 1) °C modified the bias in GOS surface water temperature by 0.65(− 1.12) °C similarly all over the study area. These results indicate that the surface heating near the Straits of Gubal is dominated by the exchange through the Straits of Gubal rather than by the atmospheric forcing, while over the central and northern GOS the atmospheric forcing dominates the exchange process.

3.2.2 Spatial Distribution

Water level over the GOS shows average annual values of $-1.4\times\times10^{2}\pm0.02$ m over mean sea level with significant seasonal variations ranging from $-6.7\times10^{2}\pm0.02$ m during winter to $4.3\times10^{2}\pm0.02$ m during summer (Fig. 11), partly due to the water balance of GOS. Water level increased from south to north over GOS and exhibited significant annual spatial ranges from -6×10^{-2} to 0.5×10^{-2} m.

The spatial distribution of predicted SST and vertical profiles of water temperature was also studied. GOS SST averaged annual values of 23 ± 0.86 °C were found, with marked seasonal variations ranging from 25.78 ± 0.56 °C for summer average to 20.37 ± 1.85 °C for winter average (Fig. 12). The SST distributions show a meridional pattern increasing from north to south, partly due to total heat loss to the atmosphere. The only exception is during summer when SST over the central GOS is much warmer than at southern and northern GOS, partly due to the effect of surface $T2$ m. It is clear that the southern part of GOS is highly affected by the water input from the Red Sea, while the northern and central GOS are profoundly affected by the forcing process (as mentioned before on the sensitivity runs).

To examine the GOS stratification conditions and 3-D temperature structure, time series of average spatial water temperature at different depths (0, 30, and 75 m) are shown in Fig. 13. The surface layer is subjected to higher variance in values compared with other values, partly due to the effect of atmospheric conditions. During winter and autumn, the stratification is very low (the difference between the upper and bottom layer is generally less than 0.5 °C) while

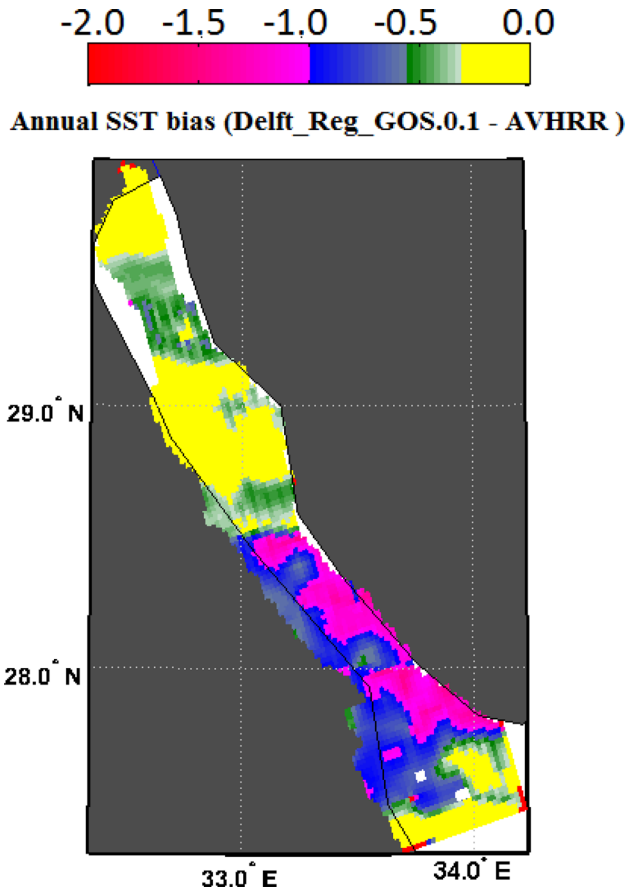

Fig. 9 Annual bias between Delft_Reg_GOS.0.1 and AVHRR SST over the Gulf of Suez

it is significant during summer and spring (the difference between the upper and bottom layer exceeds 1.5 °C).

Evaporation rate over GOS was also analyzed and averaged annual values of -8.02 ± 0.97 mm/day were found, with marked seasonal variations ranging from -7.4 ± 1.17 mm/day during winter to -8.56 ± 1.11 mm/day during summer (Fig. 14). The annual evaporation rate of 8 mm/day induces 2.8 m water loss of GOS during 1 year. This water loss must be balanced by the net water flowing to GOS, precipitation rates, and water level changes as follow:

$$A_s \frac{\partial \eta}{\partial t} = Q_{in} - Q_{out} + A_s(\text{Tp} - \text{Evaporation}) + Q_f,$$

where A_s is the GOS surface area ($=7948.872 \times 10^6$ m^2), $\frac{\partial \eta}{\partial t}$ is the change in sea level with time, Q_{in} (Q_{out}) is the inflow (outflow) water throw the Straits of Gubal, and Q_f the river discharge to the basin ($=0$ over GOS).

It is clear that the water balance in GOS is controlled by the water exchange through the Straits of Gubal (Q_{in} and Q_{out}), and by net precipitation, i.e., the difference between the precipitation and evaporation rates. The various water balance components, except precipitation, are modeled using the Delft_Reg_GOS.0.1. The described exchange through the Straits of Gubal (data not shown) reveals an annual average inflow of 0.1617 Sv and an annual average outflow of 0.1610 Sv. Moreover, Table 2 shows the estimated seasonal and annual mean of the difference between inflow and outflow (hereafter Q_o) and the net precipitation flow, i.e., $A_s(P-E)$.

3.2.3 Exchange Characteristics Through Straits of Gubal and Depth-Averaged Circulation

3.2.3.1 Exchange Through the Straits of Gubal Figure 15 depicts the most important water route systems between the Gulf of Suez and the Red Sea through the Straits of Gubal. These routes show a significant change from layer to layer. Over the upper four layers, the direction of the flow shows a marked outflow to the Red Sea, in particular through the

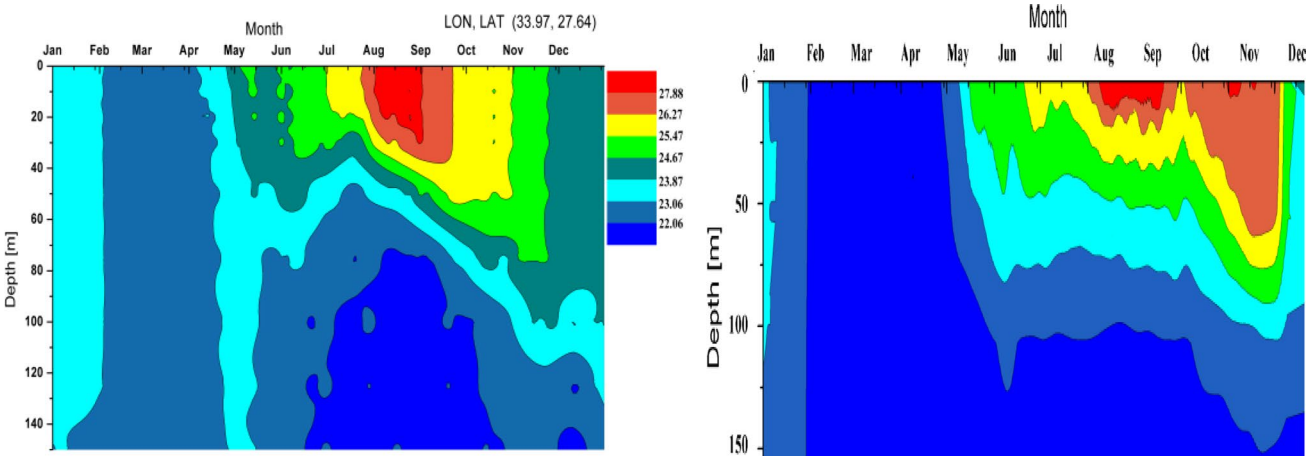

Fig. 10 Time series of modeled (left panel) and World Ocean Atlas 2013 (right panel) water temperature profiles at a model station (27.6°N, 34.1°E) south of the Straits of Gubal

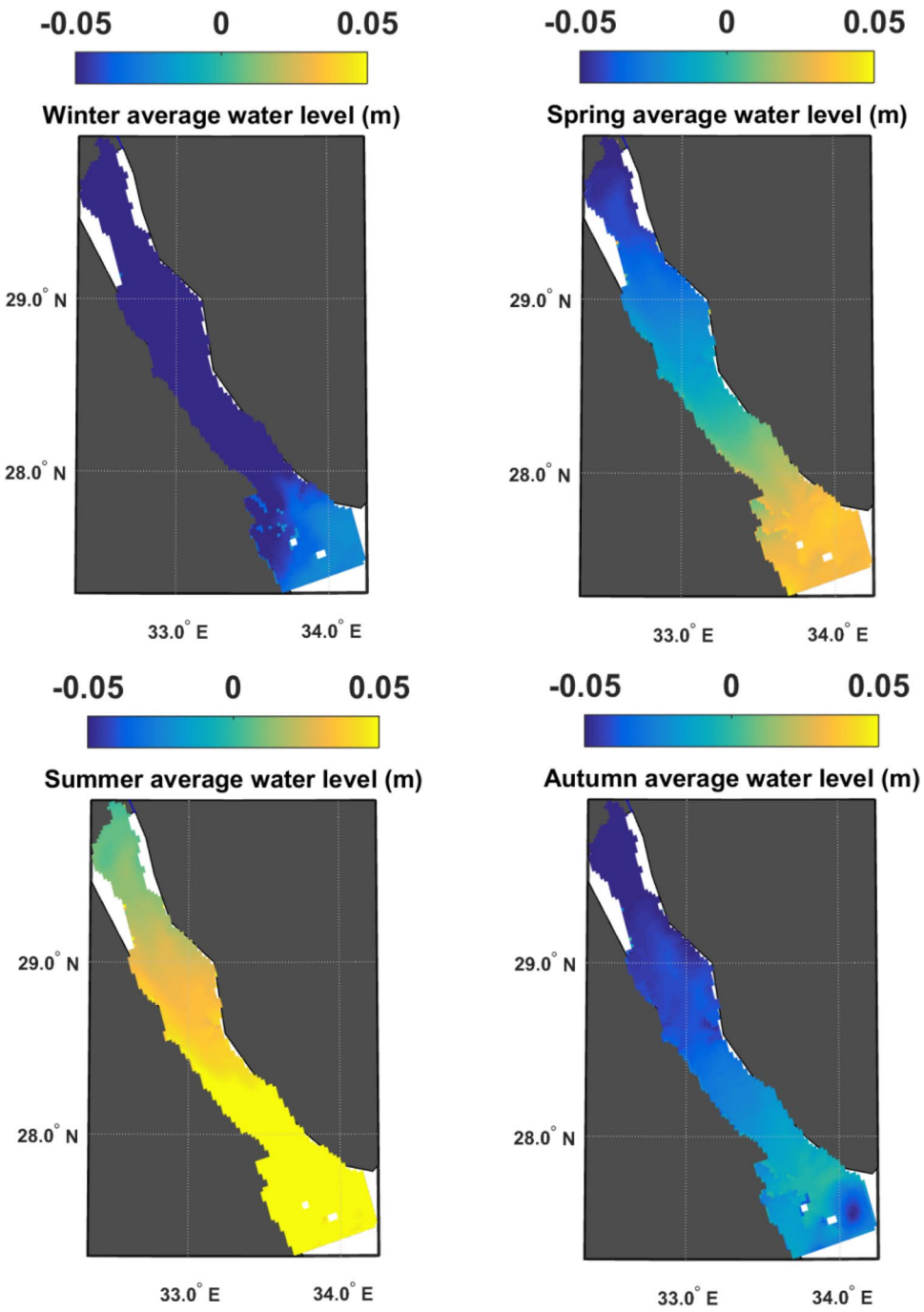

Fig. 11 Spatial distribution of averaged seasonal water level over 2013

western side of the Straits of Gubal. From layer 5 to layer 10, the western outflow is still significant, but with lower speeds compared to the upper four layers. Moreover, a reversed inflow route started to develop along the middle of the Straits of Gubal and associated with well-defined cyclonic eddies over the southeastern side of the GOS. From layer 10 to the bottom, the outflow system becomes dominant over the inflow system.

3.2.3.2 Depth-Averaged Circulation over the Gulf of Suez The depth-averaged velocity shows significant seasonal variations (Fig. 16) reaching maximum velocities during the springtime along the western coast. Figure 16 confirms the dominant western current (always moving towards south) through the shallower coastal parts, while there are some well-formed eddies with northward net transport over the middle of the Gulf through most of the year.

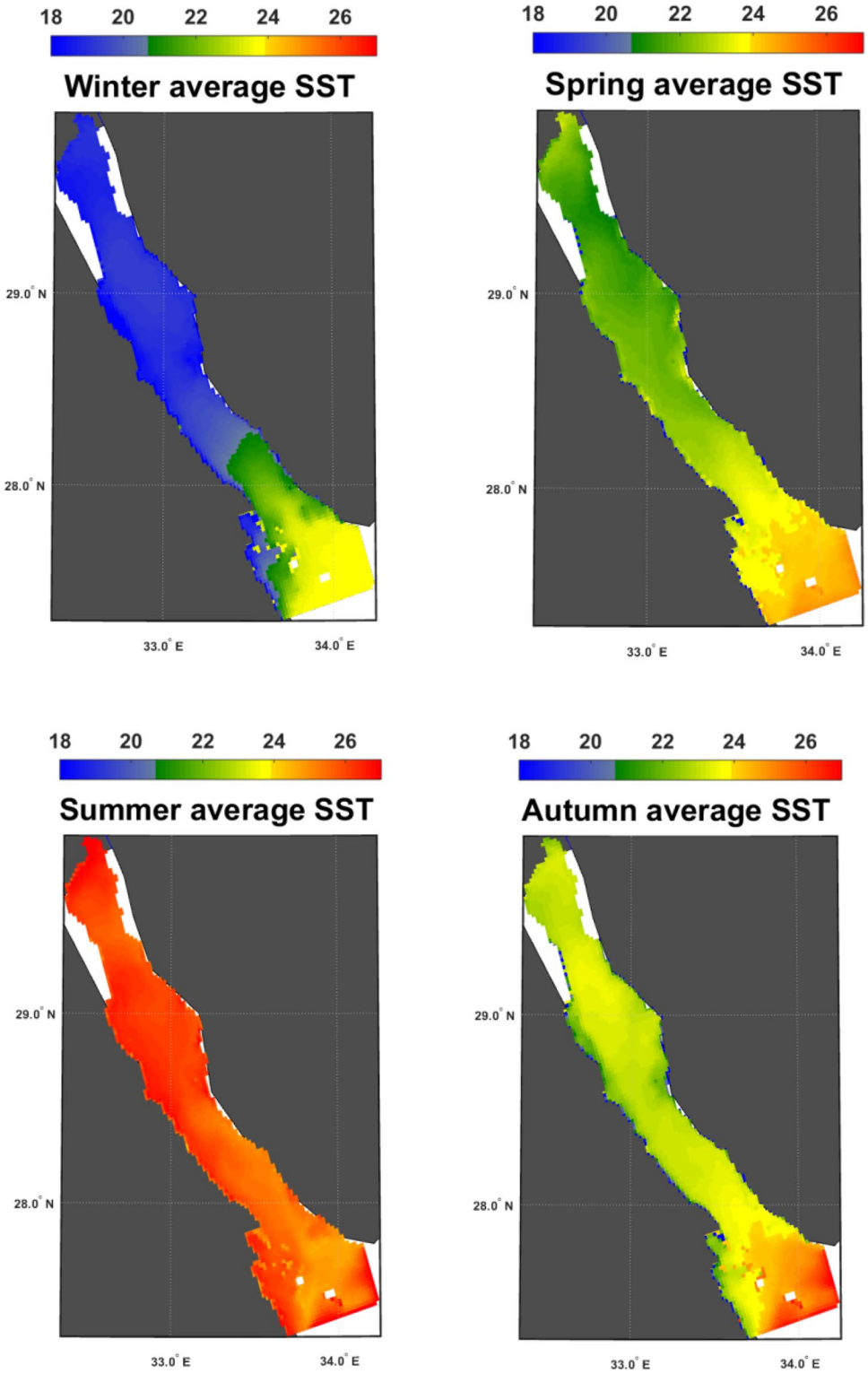

Fig. 12 Spatial distribution of averaged seasonal SST (°C) over 2013

During winter, the depth-averaged current ranged from calm to 0.2 m/s. The maximum winter depth-averaged velocity occurred over the cyclonic gyre which is located over the southeastern entrance of GOS (Fig. 16a). During spring, a dominant current (moving northward) starts to develop along the middle part of the GOS with the enhanced western direction (moving southward). In addition, the cyclonic gyre at the southwestern entrance of the GOS is migrating south simultaneously with the generation of a well-formed anti-cyclonic gyre to the north

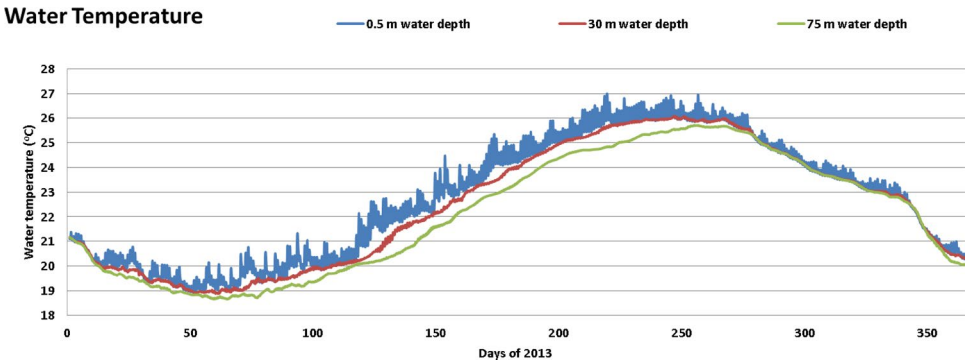

Fig. 13 Spatially averaged water temperature profiles at different depths of Gulf of Suez over 2013

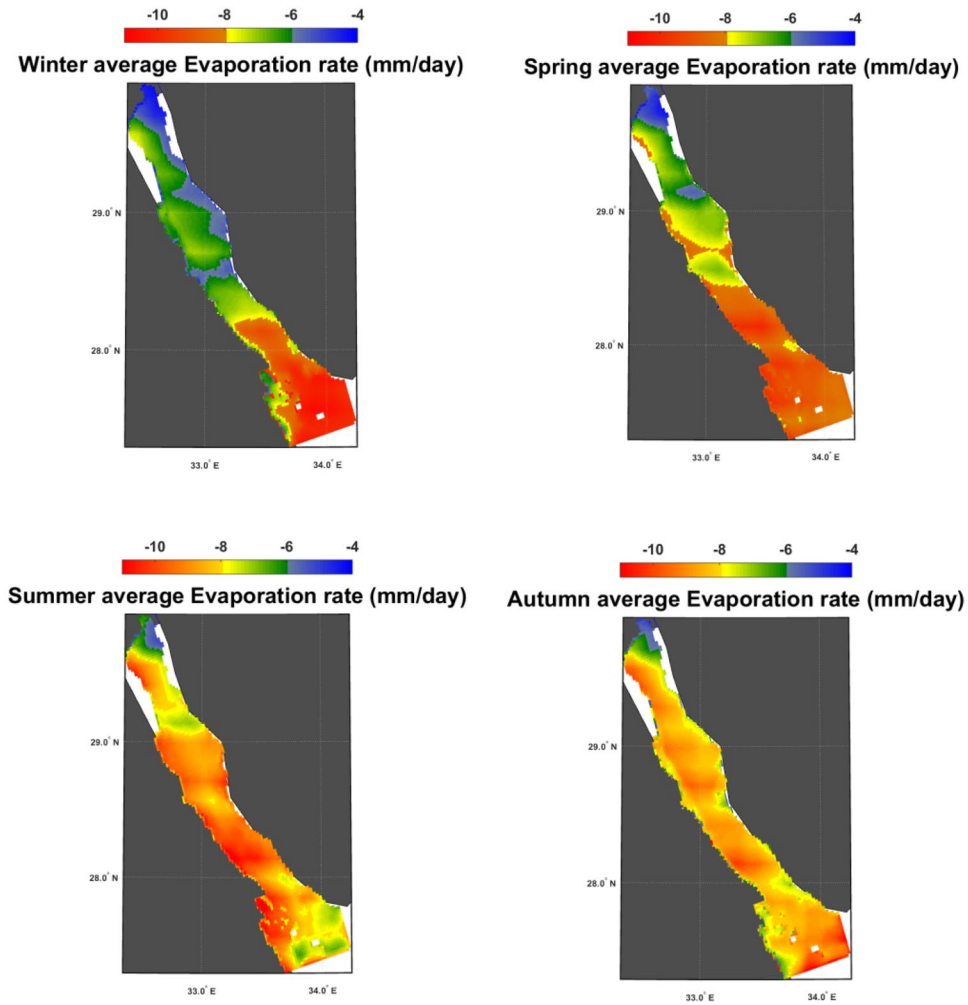

Fig. 14 Gulf of Suez's seasonal surface evaporation rate (mm/day) distributions

(Fig. 16b). During summer, the gyre system located southwestern to the entrance of the GOS has three gyres. In addition, the western current (moves southward) becomes less significant. During autumn, the gyre system located southwestern to the entrance of the GOS integrates two anti-cyclonic gyres associated with the cyclonic gyre.

4 Summary and Conclusion

The modeling system presented here mainly depends on the one-way coupling from the atmospheric model (RegCM 4) to force the near-shore hydrodynamic models

Table 2 Modeled seasonal and annual mean water balance of the Gulf of Suez over 2013

	A_s (Tp-evaporation) [10^6 m^3 s^{-1}]	Qo(= $Q_{in} - Q_{out}$)	$A_s \frac{\partial \eta}{\partial t}$
Winter	− 0.00066	0.00099	0.00034
Spring	− 0.00070	0.00027	− 0.00043
Summer	− 0.00075	0.00083	0.00008
Autumn	− 0.00073	0.00069	− 0.00004
Annual	− 0.00071	0.00070	− 0.00001

(Delft3D) via the connection between atmospheric conditions over the GOS Basin and its local oceanic features during 2013.

The individual terms of the water level, water temperature, evaporation, and water balances were analyzed together with the exchange through the Straits of Gubal and depth-averaged circulation. Delft_Reg_GOS.0.1 predictions well-follow the observations and the results showed strong seasonal variations in all the studied components.

Using HYCOM modeling results across the open boundary, together with the parametrization of the initial condition and the buffer zone to the south of the GOS, the exchanges through the Straits of Gubal were realistically predicted. The calculated net water flow (0.00070×10^6 m^3 s^{-1}) to the GOS was in dynamical balance with the net precipitation rates (-0.00071×106 m^3 s^{-1}), resulting in a total loss of water level over the GOS of approximately 3.9×10^{-3} m. Generally, the Delft_Reg_GOS.0.1 model calculations of the outflow through the Strait of Gubal (0.1610 Sv) support the previous finding by Rady et al. (2000) and Maillard (1972).

Water level annual spatial variations show a range of 6.5×10^{-2} m and gradually decrease from south to north over the GOS, in counter to the dominant wind direction, anticipating a complex water circulation over the GOS.

Surface water temperature decreases gradually from south to north over the GOS, showing a spatial variation range of 5.2 °C. According to the four sensitivity runs performed, the warming process near the Straits of Gubal depends on warm-water advection from the Northern Red Sea, while the mixing induced by atmospheric conditions is responsible for the heating over the central and northern GOS. This runs in counter to the adjacent basin, the Gulf of Aqaba (Biton and Gildor 2011), where the input from the Red Sea induces the heating overall in the Aqaba Gulf. This different behavior between the two adjacent gulfs can be explained by the deeper depth of Aqaba Gulf compared to GOS. Over the GOS (shallow area), the combined effect of heat flux and wind speed controls the process of stratification. The layers are well-mixed during winter and spring seasons and stratification is generated at low wind speeds and high surface heat flux (summer time).

The GOS circulations are characterized by a complex system integrating: (1) western current (moved to south), (2) gyre system over the southeastern part of the study area (including two gyres: one anti-cyclonic and other cyclonic), and (3) some eddies along the middle GOS, with net north water movements. This complex system with net surface outflow confirms the previous findings of the surface heating effect over the central and northern GOS which significantly depends on the mixing process with the atmosphere. Due to the lack of observations and scientific literature, the model predictions about the local circulations could not be validated.

Finally, the Delft_Reg_GOS.0.1 model proved to be a promising tool to predict and study the environmental issues over the GOS (e.g., frequent oil spill events, biogeochemical cycle, etc.). Long-term features of the GOS Basin merit our consideration and will be discussed in the future. Moreover, two-way coupling merits our interest and will be applied in the upcoming modeling version.

Moreover, the current research highlighted the need for more local field measurements, such as CTD measurements in the Gulf of Suez to further validate the model. Systematic monitoring of the Gulf of Suez mouth is essential to understand its response to atmospheric forcing as well as to quantify the exchange between the GOS and the Red Sea.

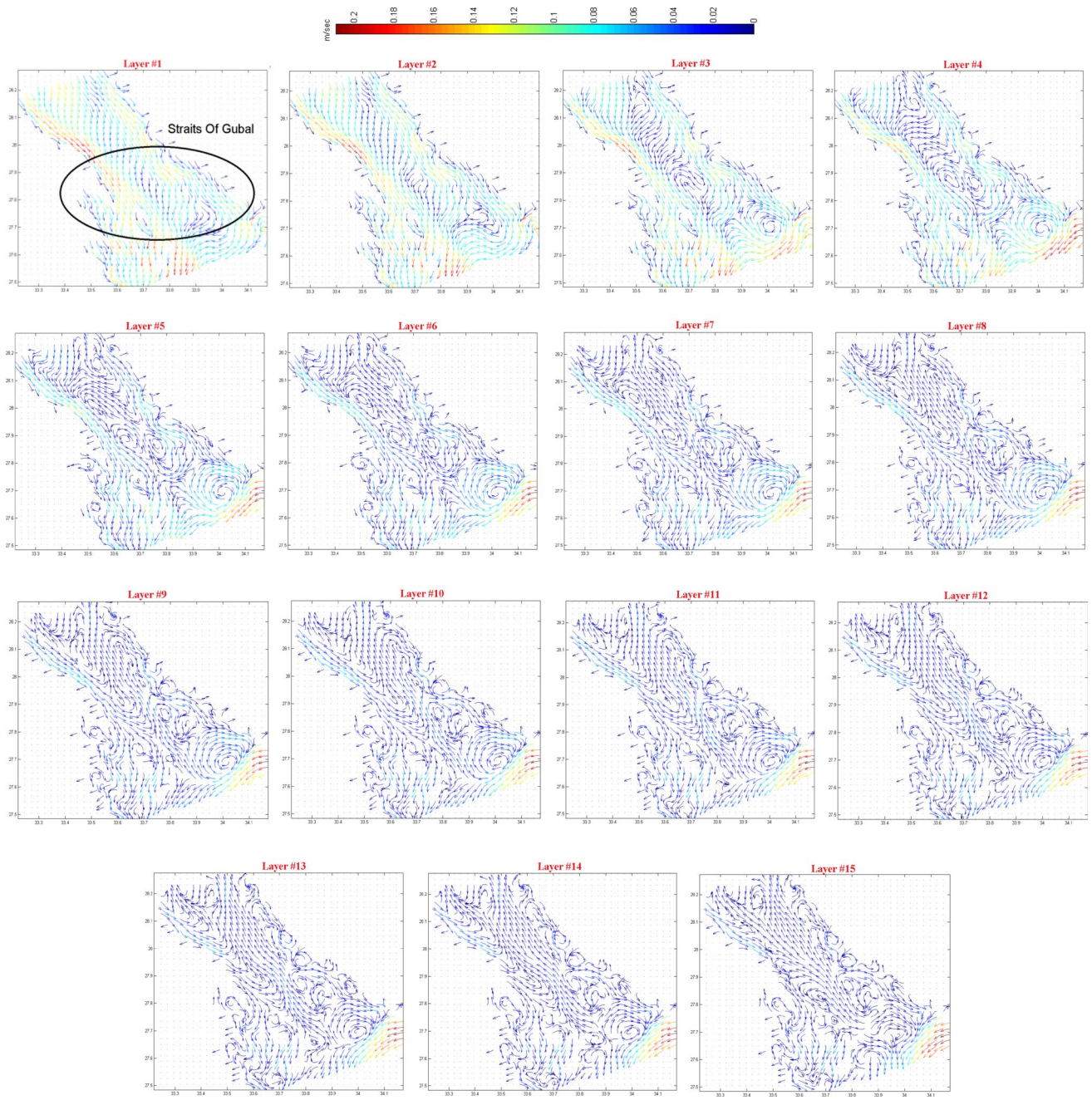

Fig. 15 Modeled water current speeds (m/s) near the Straits of Gubal over the 15 studied layers (arrow length increases linearly with increasing current speed). These dates were selected to illustrate the most important transport systems between the Gulf of Suez and the Red Sea

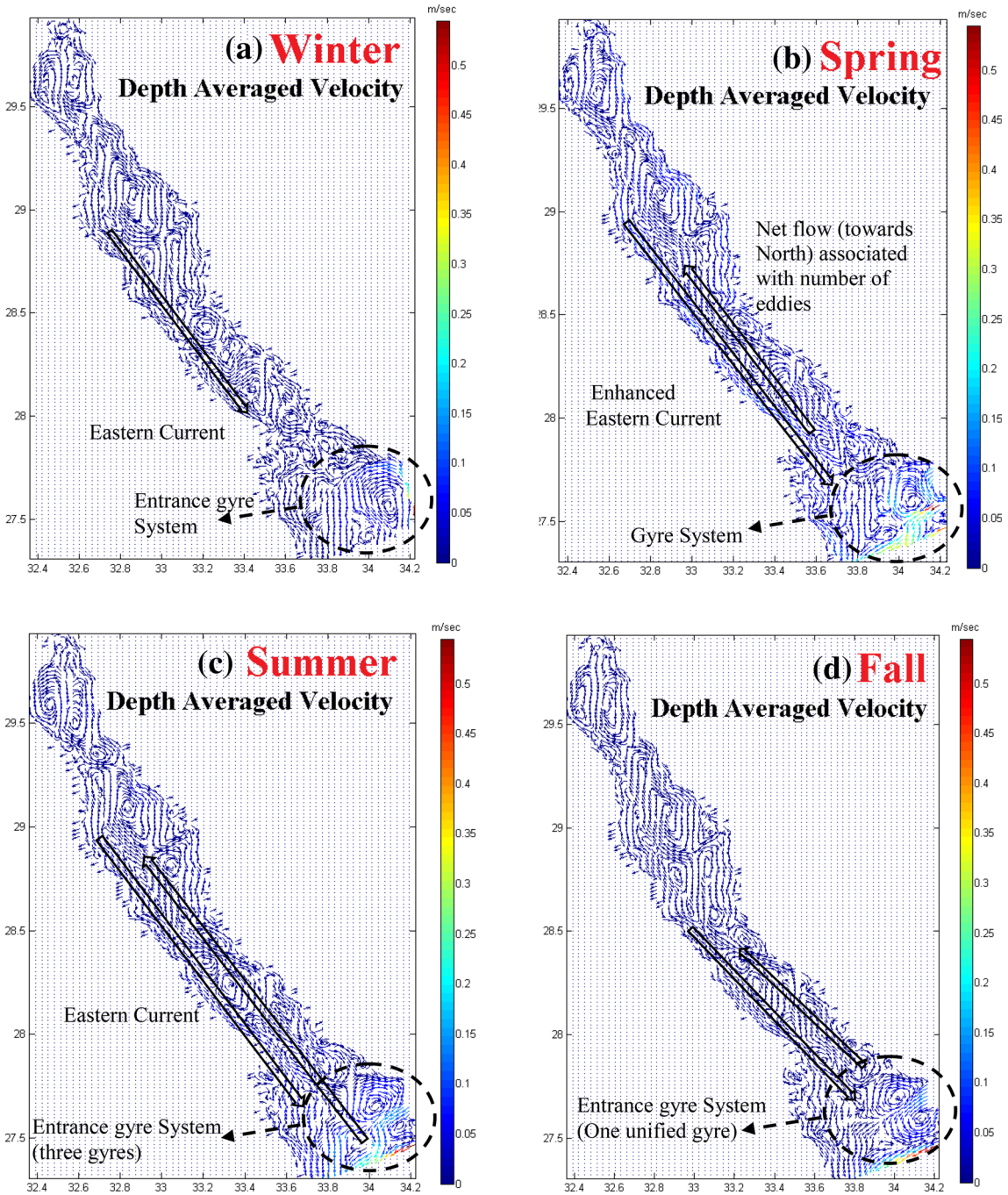

Fig. 16 Seasonal averaged depth currents (m/s) and dominant currents direction and gyres over Gulf of Suez

Acknowledgements The first author is supported by a scholarship from the Mission Department, Ministry of Higher Education of the Government of Egypt which is gratefully acknowledged. The third author of this work has been supported by the Portuguese Science Foundation (FCT) through a postdoctoral Grant (SFRH/BPD/99707/2014). This study was partially supported by the National Foundation for Science and Technology-FCT, through CESAM (UID/AMB/50017/2013). This research was undertaken when Mr. Ahmed Eladawy was a visiting junior researcher at Nadaoka lab (Tokyo Institute of Technology). Lawrence Patrick BERNARDO (Tokyo Institute of Technology) and Sommer Abdel-Fattah (E-JUST) are acknowledged for their efforts on revising the manuscript. We are grateful to the National Climatic Data Center (NCDC) and National Oceanic and Atmospheric Administration (NOAA) for providing the remotely sensed datasets through their websites.

References

Abualnaja Y, Papadopoulos VP, Josey SA, Hoteit I, Kontoyiannis H, Raitsos DE (2015) Impacts of climate modes on air–sea heat exchange in the Red Sea. J Clim 28:2665–2681. https://doi.org/10.1175/JCLI-D-14-00379.1

Adcroft A, Campin J, Dutkiewicz S, Evangelinos C, Ferreira D, Forget G et al (2016) MITgcm user manual, pp 1–485, Chicago. http://mitgcm.org/public/r2_manual/sav_docs_20140901_1544/online_documents/manual.html

Al Gain A, Clark J, Chiffings T (1987) A coastal management program for the Saudi Arabian Red Sea coast. In: Coastal Zone'87, pp 1673–1681. ASCE. http://cedb.asce.org/CEDBsearch/record.jsp?dockey=0051840

Barakat AO, Mostafa AR, Qian Y II, Kennicutt li MC (2002) Application of petroleum hydrocarbon chemical fingerprinting in oil spill investigations—Gulf of Suez, Egypt. Spill Sci Technol Bull 7(5–6):229–239

Biton E, Gildor H (2011) The general circulation of the Gulf of Aqaba (Gulf of Eilat) revisited: the interplay between the exchange flow through the Straits of Tiran and surface fluxes. J Geophys Res Ocean. https://doi.org/10.1029/2010JC006860

Bentamy A, Fillon DC (2012) Gridded surface wind fields from Metop/ASCAT measurements. Int J Remote Sens 33(6):1729–1754. https://doi.org/10.1080/01431161.2011.600348

Bower AS (2002) Gulf of Aden eddies and their impact on Red Sea Water. Geophys Res Lett 29:2025. https://doi.org/10.1029/2002GL015342

Bye JAT (1996) Coupling ocean–atmosphere models. Earth-Sci Rev 40:149–162. https://doi.org/10.1016/0012-8252(95)00050-X

Calmanti S, Artale V, Sutera A (2006) North Atlantic MOC variability and the Mediterranean Outflow: a box-model study. Tellus A 58:416–423

Cember RP (1988) On the sources, formation, and circulation of Red Sea deep water. J Geophys Res Ocean 93:8175–8191

Chang R, Rong Z, Badger M, Hasager CB, Xing X, Jiang Y (2015) Offshore wind resources assessment from multiple satellite data and WRF modeling over South China Sea. Remote Sens 7:467–487. https://doi.org/10.3390/rs70100467

Chassignet EP, Hurlburt HE, Smedstad OM, Halliwell GR, Hogan PJ, Wallcraft AJ, Baraille R, Bleck R (2007) The HYCOM (hybrid coordinate ocean model) data assimilative system. J Mar Syst 65:60–83

Dickinson RE, Henderson-Sellers A, Kennedy PJ (1993) Biosphere-atmosphere Transfer Scheme (BATS) Version 1e as Coupled to the NCAR Community Climate Model. NCAR Technical Note NCAR/TN- 387+STR. https://doi.org/10.5065/D67W6959

Egbert GD, Erofeeva SY (2002) Efficient inverse modeling of barotropic ocean tides. J Atmos Ocean Technol 19:183–204

Egbert GD, Bennett AF, Foreman MGG (1994) TOPEX/POSEIDON tides estimated using a global inverse model. J Geophys Res Oceans 99(C12):24821–24852

Eladawy A, Nadaoka K, Negm A, Abdel-Fattah S, Hanafy M, Shaltout M (2017) Characterization of the northern Red Sea's oceanic features with remote sensing data and outputs from a global circulation model. Oceanologia 59(3):213–237. https://doi.org/10.1016/j.oceano.2017.01.002

Giorgi F (2006) Climate change hot-spots. Geophys Res, Lett, p 33

Giorgi F, Anyah RO (2012) The road towards RegCM4. Clim Res 52:3–6

Giorgi F, Mearns LO (1999) Introduction to special section: regional climate modeling revisited. J Geophys Res Atmos 104:6335–6352

Giorgi F, Coppola E, Solmon F, Mariotti L, Sylla MB, Bi X, Elguindi N, Diro GT, Nair V, Giuliani G et al (2012) RegCM4: model description and preliminary tests over multiple CORDEX domains. Clim Res 52:7–29

Grell GA (1993) Prognostic evaluation of assumptions used by cumulus parameterizations. Mon Weather Rev 121:764–787

Grell GA, Dudhia J, Stauffer DR (1994) A description of the fifth-generation Penn State/NCAR Mesoscale Model (MM5). NCAR Technical Note NCAR/TN-398+STR. https://doi.org/10.5065/D60Z716B

Hamed MA, Emara AM (2006) Marine molluscs as biomonitors for heavy metal levels in the Gulf of Suez, Red Sea. J Mar Syst 60:220–234. https://doi.org/10.1016/j.jmarsys.2005.09.007

Holtslag AAM, De Bruijn EIF, Pan HL (1990) A high resolution air mass transformation model for short-range weather forecasting. Mon Weather Rev 118:1561–1575

Hydraulics D (2006) Delft3D-FLOW user manual. Delft, The Netherlands

Hydraulics D (2011) Delft3D-Flow user manual: Simulation of multi-dimensional hydrodynamic and transport phenomena, including sediments. In: Hydro-morphodynamics

Hydraulics D (2014) Delft3D-FLOW User Manual: Simulation of multi-dimensional hydrodynamic flows and transport phenomena, including sediments. Technical report

Kiehl JT, Hack JJ, Bonan GB, Boville BA, Briegleb BP (1996) Description of the NCAR Community Climate Model (CCM3). Technical Note. No. PB–97-131528/XAB; NCAR/TN–420-STR. National Center for Atmospheric Research, Climate and Global Dynamics, Boulder, CO (United States)

Lane A (1989) The heat balance of the North Sea. http://noc.ac.uk/publication/3872

Ličer M, Smerkol P, Fettich A, Ravdas M, Papapostolou A, Mantziafou A, Strajnar B, Cedilnik J, Jeromel M, Jerman J, Petan S, Sofianos S (2016) Modeling the ocean and atmosphere during an extreme bora event in northern Adriatic using one-way and two-way atmosphere–ocean coupling. Ocean Sci 12:71–86. https://doi.org/10.5194/os-12-71-2016

Madah F, Mayerle R, Bruss G, Bento J et al (2015) Characteristics of Tides in the Red Sea Region, a Numerical Model Study. Open J Mar Sci 5:193

Maillard C (1974) Eaux intermediaires et formation d'eau profonde en MerRouge. In: L'oceanographie physique de la Mer Rouge, Centre national pour l'Exploitation des Oceans, Paris, pp 105–133

Maillard C, Soliman G (1986) Hydrography of the Red-Sea and exchanges with the Indian-Ocean in summer. Oceanol Acta 9:249–269

Morcos SA (1970) Physical and chemical oceanography of the Red Sea. Ocean Mar Biol Ann Rev 8:73–202

Murakami M, Oonishi Y, Kunishi H (1985) A numerical simulation of the distribution of water temperature and salinity in the Seto Inland Sea. J Oceanogr Soc Jpn 41:213–224

Pal JS, Eltahir EAB, Small EE (2000) Simulation of regional-scale water and energy budgets—representation of subgrid cloud and precipitation processes within RegCM. J Geophys Res 105:29579–29594

Papadopoulos VP, Abualnaja Y, Josey SA, Bower A, Raitsos DE, Kontoyiannis H, Hoteit I (2013) Atmospheric forcing of the winter air–sea heat fluxes over the northern Red Sea. J Clim 26:1685–1701. https://doi.org/10.1175/JCLI-D-12-00267.1

Pokavanich T, Alosairi Y, de Graaff R, Morelissen R, Verbruggen W, Al-Refail K, Taqi A, Al-Said T (2014) Three-dimensional hydro-environment characterization and modeling of the northern Arabian Gulf. Coast Eng Proc 1:41

Qian J-H (2008) Why precipitation is mostly concentrated over islands in the Maritime Continent. J Atmos Sci 65:1428–1441

Qian J-H, Robertson AW, Moron V (2010) Interactions among ENSO, the monsoon, and diurnal cycle in rainfall variability over Java, Indonesia. J Atmos Sci 67:3509–3524

Rady MA, El-sabh MI, Murty TS, Backhaus JO (1998) Residual circulation in the Gulf of Suez, Egypt. Estuarine Coastal Shelf Sci 46(2):205–220. https://www.sciencedirect.com/science/article/pii/S0272771497902729

Rasul NMA, Stewart ICF (2015) The Red Sea: the formation, morphology, oceanography and environment of a young ocean basin. Springer, New York

Roberts PJW, Villegas B, Morelissen R (2015) Coupling a near field outfall model with a far field hydrodynamic model. In: 36th IAHR World Congress, pp 1–10

Shaltout M, Omstedt A (2015) Modelling the water and heat balances of the Mediterranean Sea using a two-basin model and available meteorological, hydrological, and ocean data. Oceanologia 57:116–131. https://doi.org/10.1016/j.oceano.2014.11.001

Shchepetkin AF, McWilliams JC (2005) The regional oceanic modeling system (ROMS): a split-explicit, free-surface, topography-following-coordinate oceanic model. Ocean Model 9:347–404

Towers JR (2015) The Red Sea the formation, morphology, oceanography and environment of a young ocean basin. J Near East Stud. https://doi.org/10.1086/371522

Twigt DJ (2006) 3D temperature modeling for the South China Sea using remote sensing data, MSc. Thesis report, WLDelft Hydraulics and Delft University of Technology

van den Heuvel S (2010) Modeling the hydrodynamics and salinity of the Pontchartrain Basin. MSc-thesis. Delft University of Technology

Watterson IG, Syktus J (2006) The influence of air–sea interaction on the Madden–Julian Oscillation: the role of the seasonal mean state. Clim Dyn 28:703–722. https://doi.org/10.1007/s00382-006-0206-9

Woelk S, Quadfasel D (1996) Renewal of deep water in the Red Sea during 1982–1987. J Geophys Res Ocean 101:18155–18165

Woolnough SJ, Vitart F, Balmaseda MA (2007) The role of the ocean in the Madden–Julian Oscillation: implications for MJO prediction. Q J R Meteorol Soc 133:117–128. https://doi.org/10.1002/qj.4

Wyrtki K (1974) Sea level and the seasonal fluctuations of the equatorial currents in the western Pacific Ocean. J Phys Oceanogr 4:91–103

Yao F, Hoteit I, Pratt LJ, Bower AS, Zhai P, Köhl A, Gopalakrishnan G (2014) Seasonal overturning circulation in the Red Sea: 1. Model validation and summer circulation. J Geophys Res Ocean 119:2238–2262

Zeng X, Zhao M, Dickinson RE (1998) Intercomparison of bulk aerodynamic algorithms for the computation of sea surface fluxes using TOGA COARE and TAO data. J Clim 11:2628–2644